Collective ballistic motion explains fast aggregation in adhesive active matter

Emanuel F. Teixeira,[1,*] P. de Castro,[2,†] Carine P. Beatrici,[1,‡]
Heitor C. M. Fernandes,[1,§] and Leonardo G. Brunnet[1,¶]

[1] *Instituto de Física, Universidade Federal do Rio Grande do Sul, CP 15051, CEP 91501-970 Porto Alegre - RS, Brazil*
[2] *ICTP South American Institute for Fundamental Research, Instituto de Física Teórica, UNESP – Universidade Estadual Paulista, Rua Dr. Bento T. Ferraz 271, 01140-070, São Paulo, SP, Brazil*

(Dated: September 9, 2025)

Inspired by motile cells in tissue formation, we find that active systems of self-aligning adhesive particles undergo ballistic aggregation through a flocking transition. This kinetic regime emerges when the cluster persistence length grows faster with cluster mass than the intercluster distance does. We also identify and explain distinct non-collective kinetic regimes, including biologically relevant long-lived transients. Our analytical and numerical results offer a unified framework explaining the broad range of experimentally observed aggregation exponents in cellular systems and reveal physical principles potentially critical for timely tissue organization.

Introduction—Aggregation processes are ubiquitous, from aerosols to living matter [1–5]. In active systems, motile cells can agglomerate, driving phenomena like bacterial biofilm initiation [6, 7] and tissue formation [8]. In particular, there has been long-standing interest in cell-sorting experiments [9–11], where cells clusters meet and grow by successive mergers [9–11]. In these systems, strong cell–cell adhesion suppresses cluster fragmentation. Yet, complex interactions and motion generate rich aggregation kinetics that remain elusive despite their key role in timely tissue organization [12].

In diffusion-limited cluster aggregation (DLCA), clusters move diffusively with a diffusivity that decreases inversely with cluster mass [13]. This classical picture predicts that in two dimensions, without cluster fragmentation, the average cluster mass grows as $\overline{M}(t) \sim t^z$ with an aggregation exponent $z = 1/2$ [14–16]. In contrast, ballistic cluster motion yields $z \simeq 1$, provided that self-propulsions are uncorrelated between cells [13, 17, 18]. However, experiments in active tissues report faster coarsening dynamics with $z > 1$ [12], indicating that classical models are insufficient.

Motivated by these discrepancies, Mones et al. [19] simulated adhesive active particles with self-alignment [20], where self-propulsion gradually aligns with the particle's net velocity, obtaining $z \simeq 2$. This rapid coarsening was attributed to collective motion, akin to Vicsek-like systems [15, 21, 22], but its mechanistic origin remained unexplained. Subsequently, Beatrici et al. [23] showed how internal cluster alignment alters the diffusivity-mass relation, modifying z; however, their analysis was limited to weak alignment and persistence, yielding at most $z = 1$.

In this work, we show that the anomalous exponent $z \simeq 2$ arises because, as a consequence of flocking, the cluster persistence length grows linearly with cluster mass, while the intercluster distance scales as the square root of mass. This corresponds to a crossover into the regime termed here collective ballistic aggregation (CBA). Our analysis relies on simulations of adhesive active particles, in which we varied both particle persistence and self-alignment strength. Beyond CBA, we also elucidate other mechanisms underlying a broad range of experimental aggregation exponents. Our results are supported by analyses of single-cluster dynamics and a generalized Smoluchowski coagulation theory [24]. The present work unifies disparate experimental and theoretical observations and shows how cooperative behavior reshapes aggregation kinetics in living matter.

Model—We employ a minimal model inspired by motile tissue cells [25] with particles represented as disks subject to contact forces and self-alignment: each particle self-propels along a noisy direction that gradually aligns with its own net velocity. A strong attractive force accounts for cell adhesion. Self-alignment induces collective motion and is more realistic in this context than the original Vicsek alignment [26], since tissue cells cannot explicitly average over neighbors [25]. Our results are robust to the choice of alignment rule, as observed for Vicsek-like alignment at low strength [23].

We consider N adhesive active Brownian disks in 2D with periodic boundary conditions [25, 27]. Their dynamics is given by

$$\dot{\mathbf{r}}_i = v_0\,\mathbf{n}_i + \mu \sum_{j\neq i} \mathbf{F}_{ij}\,, \tag{1}$$

$$\dot{\theta}_i = -J\frac{\partial}{\partial\theta_i}\left(\mathbf{n}_i\cdot\hat{\mathbf{v}}_i\right) + \sqrt{2D_R}\,\xi_i\,, \tag{2}$$

where v_0 is the self-propulsion speed, $\mathbf{n}_i = (\cos\theta_i, \sin\theta_i)$ is the self-propulsion direction, also called polarity, ξ_i is a Gaussian white noise with $\langle \xi_i(t)\xi_j(t')\rangle = \delta_{ij}\delta(t-t')$ and $\hat{\mathbf{v}}_i = \mathbf{v}_i/|\mathbf{v}_i|$, where $\mathbf{v}_i = \dot{\mathbf{r}}_i$. Parameters D_R and J set the reorientation timescales $\tau_R = 1/D_R$ and $\tau = 1/J$, respectively. The self-alignment term has a pseudo potential $E_{\text{align}} = -J\,\mathbf{n}_i\cdot\hat{\mathbf{v}}_i$ [28, 29]. The force $\mathbf{F}_{ij}$ between particles i and j comprises a short-range repulsion and a

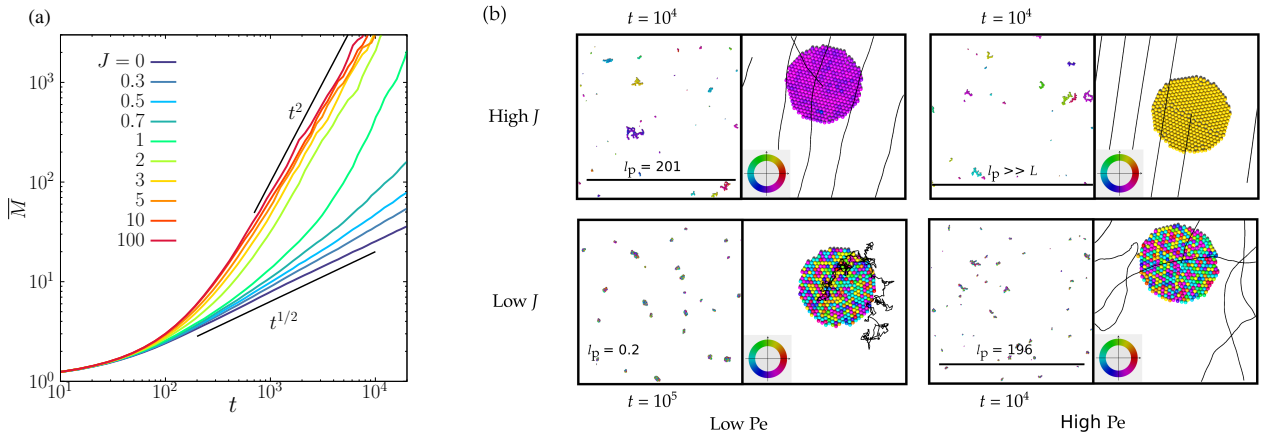

FIG. 1. Adhesive active matter exhibits rich aggregation kinetics. (a) Time evolution of the average cluster mass $\overline{M}(t)$ for different values of J. Stronger alignment accelerates aggregation and increases exponents. Here, Pe = 1. (b) Snapshots of aggregation and cluster dynamics in different regimes for low alignment ($J = 0$), high alignment ($J = 100$), low individual-particle persistence (Pe = 1) and high individual-particle (Pe = 10^3). Scale bars show cluster persistence length. Colors indicate particle polarity (see color wheel). L is the simulation box length.

short-range adhesion. For interparticle distances $|\mathbf{r}_{ij}| \leq \sigma$, a repulsive force $\mathbf{F}_{ij}^{\text{rep}} = -k_c\left(|\mathbf{r}_{ij}| - \sigma\right)\hat{\mathbf{r}}_{ij}$ accounts for overlap between the disks, where σ is their diameter and $\hat{\mathbf{r}}_{ij} = \mathbf{r}_{ij}/|\mathbf{r}_{ij}|$ is the unit vector connecting the centers of particles i and j. In the range $\sigma < |\mathbf{r}_{ij}| \leq l_{\text{adh}}$, an adhesive force $\mathbf{F}_{ij}^{\text{adh}} = -k_{\text{adh}}\left(|\mathbf{r}_{ij}| - \sigma\right)\hat{\mathbf{r}}_{ij}$ attracts neighboring particles, where l_{adh} sets the adhesive interaction range.

We measure length and time in units of σ and $\tau_0 = \sigma/v_0$, kept constant throughout this work. We thus express the polarity decorrelation time τ_R as the (rotational) Péclet number [30, 31], $\text{Pe} \equiv v_0\tau_R/\sigma = \tau_R/\tau_0$. We start from a random initial condition and let the system evolve into growing clusters by merger events where particles irreversibly adhere. Unless otherwise specified, we employ $N = 4 \times 10^4$ particles. To suppress multi-cluster mergers and percolation effects, we use a low packing fraction, $\phi = 0.01$. This produces slow aggregation kinetics (without altering the exponents) in which the cluster-mass distribution evolves more smoothly and the power-law regime is extended in time, thereby improving statistics. We also performed tests at moderately higher ϕ and observed the same exponents. Additional details are in the Supplemental Material [32].

Low particle persistence—First, we consider self-alignment in the low-Pe regime (Pe = 1). To quantify the aggregation kinetics, Figure 1a shows our results for the average cluster "mass" (i.e., the number of particles in a cluster) versus time, where a power-law behavior, $\overline{M}(t) \sim t^z$, sets in after some transient time. Between $J = 0$ and $J \approx 0.7$, the aggregation exponent changes from $z = 1/2$ to $z = 1$. Upon further increasing J, z jumps to $z \approx 2$. Snapshots of the aggregates are shown in Figure 1b; for movies, see Supplemental Material [32]. Later in this work, a comparison between intercluster distance and cluster motion persistence length will be motivated and presented.

To understand the dependence of z on J, we simulated single isolated clusters since their movement affect z. Cluster trajectories are shown also in Figure 1b; for movies of single-cluster simulations, see Supplemental Material [32]. We quantify the alignment of polarities within a cluster using the global polar order parameter, $\Psi = \left\langle \left| \sum_i^M \mathbf{n}_i \right| \right\rangle_t / M$, where $\langle ... \rangle_t$ is the steady-state average [30]. High ($\Psi \to 1$) or low ($\Psi \to 0$) collectivity reflects strong or weak alignment, respectively. Figure 2a displays Ψ versus J for different cluster masses, showing that J induces polar order [25, 26, 30, 33]. Polar order emerges as particles adhere and move together with similar velocities. At strong J, particles eventually self-align with their common velocity. The difference in Ψ between order and disorder increases with mass.

To characterize single-cluster motion, we compute the mean-squared displacement (MSD), $\left\langle \Delta r^2 \right\rangle = \left\langle \left(\mathbf{r}_{\text{cm}}(t) - \mathbf{r}_{\text{cm}}(t_0)\right)^2 \right\rangle$, where $\mathbf{r}_{\text{cm}}$ is the cluster center of mass and t_0 was set as the time after which the cluster dynamics becomes stationary. These MSD curves are well fitted by the active Brownian particle model: $\left\langle \Delta r^2 \right\rangle = 2V_c^2\tau_p\left[t - \tau_p\left(1 - e^{-t/\tau_p}\right)\right]$ [34–37], where V_c is the effective cluster self-propulsion speed, τ_p is its persistence time and we relabelled $t - t_0$ as just t. Ballistic motion occurs at short times ($t \ll \tau_p$), where $\left\langle \Delta r^2 \right\rangle \approx V_c^2 t^2$, crossing over to normal diffusion at long times ($t \gg \tau_p$), where $\left\langle \Delta r^2 \right\rangle \approx 2V_c^2\tau_p t$.

For $J = 0$ (Fig. 2b), $\left\langle \Delta r^2 \right\rangle$ decreases with cluster mass in both ballistic and diffusive regimes. Without alignment, particle polarities often oppose each other, leading

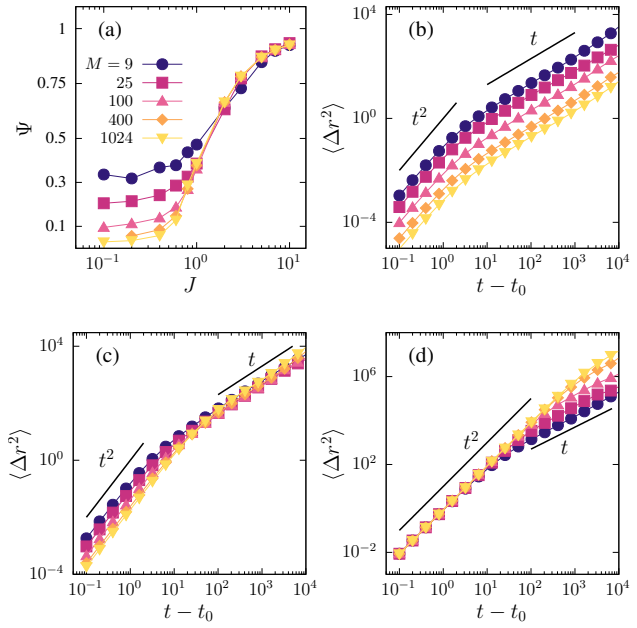

FIG. 2. Self-alignment induces a collective motion transition, altering the cluster ballistic regime duration and speed as well as the effect of cluster mass on motion. (a) Collectivity order parameter Ψ versus J for different masses. A transition occurs near $J \approx 0.6$. MSD curves, $\langle \Delta r^2 \rangle (t)$, for (b) the disordered regime ($J = 0$), (c) near the transition ($J = 0.6$), and (d) in the collective regime ($J = 10$). Here, Pe $= 1$.

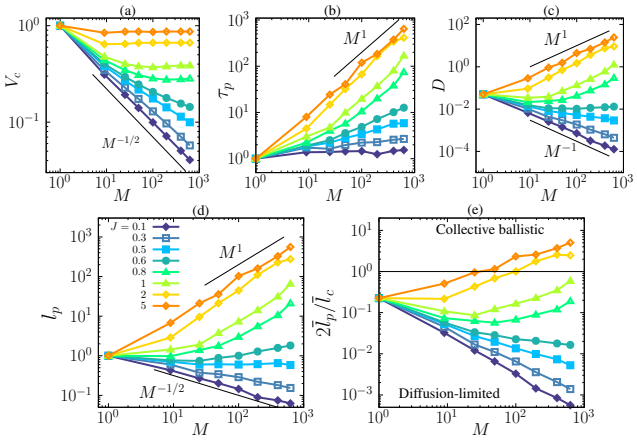

FIG. 3. Self-alignment fundamentally alters how cluster properties depend on mass, explaining aggregation kinetics regimes. For different J, the dependence on cluster mass, obtained from single-cluster simulations, is shown for (a) cluster speed V_c, (b) cluster persistence time τ_p, (c) diffusion coefficient $D = V_c^2 \tau_p / 2$, showing transition from mass-hindered to mass-enhanced diffusion, (d) persistence length $l_p = V_c \tau_p$, and (e) kinetic criterion ratio $2\bar{l}_p/\bar{l}_c$, where we estimate $\bar{l}_c$ from the global density. A crossover to ballistic aggregation occurs when $2\bar{l}_p/\bar{l}_c > 1$.

to a decrease of cluster speed with mass. The persistence time τ_p equals the single-particle value τ_R and is mass-independent since for $J = 0$ reorientations are unaffected by particle-particle interactions. Near the flocking transition ($J \approx 0.6$, Fig. 2c), V_c still decreases with mass, while alignment suppresses fluctuations and makes the cluster persistence time τ_p increase with mass. These opposing trends compensate each other, yielding convergence of all $\langle \Delta r^2 \rangle (t)$ curves at long times, where they become mass-independent. Above the transition ($J = 10$, Fig. 2d), particles align their polarities, and clusters move coherently at nearly $V_c = v_0$, making V_c mass-independent. Larger clusters retain longer τ_p, so the long-time MSD now increases with mass.

We quantify the mass-dependence of the effective active cluster motion parameters obtained from single-cluster simulations. Figure 3a shows V_c versus mass for varying J. For small J, $V_c \sim M^\gamma$ with $\gamma \simeq -1/2$, as expected for the magnitude of the average of M random vectors. As J increases, γ rises to $\gamma = 0$, giving $V_c = v_0$. Figure 3b shows the cluster persistence time τ_p versus mass. We see that τ_p grows nearly as $\tau_p \sim M^\nu$, with ν increasing from 0 to approximately 1. The long-time diffusion coefficient is $D = V_c^2 \tau_p / 2$, so $D \sim M^\alpha$, where $\alpha = 2\gamma + \nu$. Fig. 3c shows that $-1 \leq \alpha \leq 1$. For low (high) J, D decreases (increases) with mass. Notice that, for extreme values of J, we observe well-defined power-law-like dependencies on M. At intermediate J, these cluster motion parameters retain a monotonic dependence on M. Thus, we will assume power-law dependencies in our theory below in order to capture the limiting values of z, as well as its trend, as J is varied.

To characterize the aggregation regime, we compare the average intercluster distance, $\bar{l}_c$, with the cluster persistence length, $l_p = V_c \tau_p$; also, see Fig. 1b. If clusters collide and merge before traveling a persistence length, the aggregation is estimated to occur in the ballistic regime. Conversely, if clusters travel a distance larger than l_p before merging, the process is DLCA. The average intercluster distance $\bar{l}_c$ is estimated from the global particle density $\rho = N/L^2$ and the average cluster mass $\overline{M}$ via $\bar{l}_c = \sqrt{\overline{M}/\rho}$ [23].

Figure 3d shows that $l_p(M) \sim M^\delta$, with $\delta = \nu + \gamma$. Applying for $M = \overline{M}$, we define $\bar{l}_p(\overline{M}) = l_p(\overline{M}) \sim \overline{M}^\delta$ which we then compare to $\bar{l}_c$ to identify the aggregation regime. If the clusters are initially separated by a distance l_c, the simplified condition for ballistic collision reads $2l_p/l_c > 1$. Fig. 3e shows $2\bar{l}_p/\bar{l}_c$ versus $\overline{M}$. For $J \geq 2$, the curves cross the criterion $2\bar{l}_p/\bar{l}_c = 1$ at $\overline{M} \approx 10^2$, indicating a ballistic aggregation regime for large masses consistent with the faster kinetics observed for $\overline{M}$ in Fig. 1a. For lower, intermediate values of J in the range $0.8 \leq J \leq 1$, the ratio $2\bar{l}_p/\bar{l}_c$ is expected to cross 1 at larger $\overline{M}$, suggesting that ballistic behavior emerges only at later times. This is also consistent with our measurements in Fig. 1a, where the aggregation ex-

ponent of $\overline{M}$ exhibits a crossover to a faster aggregation regime with $z \simeq 2$. In contrast, for $J \leq 0.6$, the ratio $2\bar{l}_p/\bar{l}_c$ remains below 1 for all mass values, indicating that the system is in the DLCA regime throughout the whole aggregation process.

Therefore, the increase in z seen in Fig. 1a signals a shift from DLCA to ballistic aggregation. This shift is driven by collective motion within clusters, which makes the persistence length grow linearly with the average mass while the ratio $\bar{l}_p/\bar{l}_c$ scales as $\sim \overline{M}^{1/2}$. At sufficiently large $\overline{M}$, the ballistic aggregation criterion is satisfied. Notably, collective ballistic aggregation represents the asymptotic regime—not merely a transient effect.

As shall be important in our theory, we analyze the impact of J on the full cluster mass distribution $P(M,t)$ [38]; see Supplemental Material [32]. These distributions show dynamical scaling: all curves collapse onto $f(M/\overline{M}) = \overline{M}^2 P(M,t)$, consistent with irreversible aggregation scenarios [13, 39].

To explain z in each regime, we generalize Smoluchowski coagulation theory; see Supplementary Material [32]. In the DLCA regime, we use an aggregation rate $K(M,M') \sim D(M)+D(M')$ [13, 40–42]. Considering the dynamical scaling of $P(M,t)$, we obtain $z = \frac{1}{1-\alpha}$. Since $-1 \leq \alpha \leq 0$ for DLCA, this yields $\frac{1}{2} \leq z \leq 1$, matching our simulations. A similar approach applies to ballistic aggregation. We employ the aggregation rate kernel, $K(M,M') \sim |V_c(M) - V_c(M')|\,(R(M)+R(M'))$, where $R(M) \sim M^{1/2}$ is the average cluster radius [13]. We obtain $z = \frac{2}{1-2\gamma}$ [32]. For $J \geq 0.8$, ballistic aggregation occurs with mass-independent cluster speed ($\gamma = 0$), yielding $z = 2$, consistent with our simulations (Fig. 4a).

High particle persistence and diagram—For high particle persistence, Pe $= 10^3$, and $J = 0$, non-collective ballistic motion emerges. Fig. 4a shows $z \simeq 1$. As in the previous case of low Pe and $J = 0$ (Fig. 3a-b), we observed $V_c \sim M^{-1/2}$ and mass-independent $\tau_p = \tau_R$. A high Pe does not affect particle alignments, giving $\bar{l}_p = V_c\tau_p \sim 10^3/\sqrt{\overline{M}}$ and $2\bar{l}_p/\bar{l}_c \simeq 225.73\overline{M}^{-1}$ at our density. Thus, $\overline{M} < 225.73$ yields ballistic aggregation, while larger masses follow DLCA. This initial power-law during ballistic aggregation is also important as long-lived transients are relevant in biological systems due to the not-so-large number of particles. Smoluchowski theory [32] gives $z = 1$, matching simulations.

At high Pe, increasing J yields again $l_p \sim M$ and consequently $2\bar{l}_p/\bar{l}_c \sim \overline{M}^{1/2} > 1$, indicating ballistic aggregation. With mass-independent cluster speed ($\gamma = 0$, Fig. 3a), Smoluchowski theory predicts $z = 2$, matching our simulations once again. Therefore, *collective ballistic aggregation* (CBA) occurs for both low and high persistence.

Figure 4b summarizes the aggregation regimes in the Pe–J plane. At low J and Pe the system follows diffusion-limited cluster aggregation (Region I); increasing Pe at low J leads to ballistic aggregation driven by persistence without collective effects (Region II); and at high J, flocking within clusters produces coherent motion characteristic of collective ballistic aggregation (Region III).

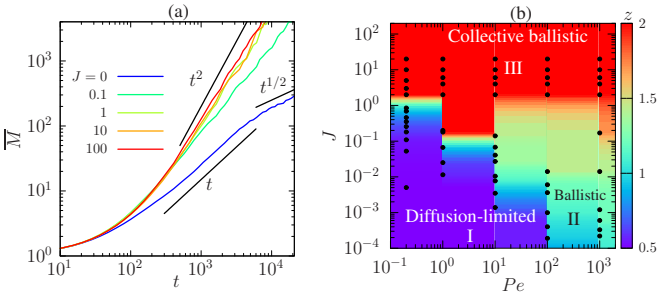

FIG. 4. High persistence enables non-collective ballistic aggregation with $z = 1$, completing the aggregation regimes. (a) $\overline{M}(t) \sim t^z$ for different J at Pe $= 10^3$. For $J = 0$, one has $z \simeq 1$ (non-collective ballistic), a long-lived transient regime relevant in biological systems, eventually crossing over to DLCA. (b) Aggregation regime diagram in terms of the aggregation exponent z. Region I (blue) is DLCA; Region II (light blue) is ballistic aggregation; Region III (red) is collective ballistic aggregation (CBA).

Conclusions—We presented a comprehensive study elucidating how collective motion enables fast cluster aggregation in adhesive active matter. Varying alignment strength (J) and Péclet number (Pe), we identified distinct regimes with scaling $\overline{M}(t) \sim t^z$, where $z \in [1/2, 2]$. Single-cluster analysis revealed how the persistence length $l_p \sim M^\delta$ emerges from the interplay between alignment and cluster size, explaining z.

At low J, clusters diffuse with an effective diffusivity that decreases with cluster mass, consistent with DLCA [14, 16]. Simulations and Smoluchowski theory yield $z \in [1/2, 1]$, matching classical DLCA. Increasing J enhances internal cluster alignment, triggering a ballistic aggregation that eventually gives $2l_p/l_c > 1$, yielding $z \approx 2$ in the high-J limit where cluster speed becomes independent of mass ($\gamma = 0$). Therefore, we identify a mechanism that allows for a *collective ballistic aggregation* regime which is asymptotic (not transient) and driven by internal alignment rather than individual persistence. Our results offer a natural explanation for the anomalous aggregation reported in prior studies [12, 19, 43]. Moreover, increasing Pe reveals that even without alignment ($J = 0$), high persistence leads to a long-lived ballistic aggregation transient, relevant to biological systems, which eventually undergoes a crossover to DLCA. After validating our simulation results through theory, we mapped all regimes in a Pe–J diagram (Fig. 4b).

Our framework elucidates how alignment and persistence govern aggregation dynamics in adhesive active matter and offers predictive insights for biological processes like tissue formation, where mass-dependent col-

lective behavior is crucial. It also explains the diversity of experimental aggregation exponents. Future work should aim to use more detailed experiments to determine the model parameters and further validate our results; to investigate high-density and cluster-fragmentation effects; and to explore how medium properties (e.g., viscoelasticity [44]) or contact inhibition [11] modulate kinetics.

We thank the Brazilian agencies CAPES, CNPq, FAPERGS and FAPESP. H.C.M.F. and L.G.B. acknowledge CNPq (procs. 402487/2023-0 and 443517/2023-1). E.F.T. acknowledges ICTP-SAIFR/IFT-UNESP. The simulations used the VD Lab cluster at IF-UFRGS. P.d.C. was supported by Scholarships No. 2021/10139-2 and No. 2022/13872-5 and ICTP-SAIFR Grant No. 2021/14335-0, all granted by São Paulo Research Foundation (FAPESP), Brazil.

* emanuel.teixeira@ufrgs.br
† pablo.castro@unesp.br
‡ carine@if.ufrgs.br
§ heitor.fernandes@ufrgs.br
¶ leon@if.ufrgs.br

[1] C. Xiong and S. Friedlander, Proceedings of the National Academy of Sciences **98**, 11851 (2001).
[2] A. A. Hyman, C. A. Weber, and F. Jülicher, Annual review of cell and developmental biology **30**, 39 (2014).
[3] S. V. Franklin and M. D. Shattuck, *Handbook of granular materials* (CRC Press, 2016).
[4] P. de Castro, F. Urbina, A. Norambuena, and F. Guzmán-Lastra, Physical Review E **108**, 044104 (2023).
[5] C. B. Caporusso, L. F. Cugliandolo, P. Digregorio, G. Gonnella, D. Levis, and A. Suma, Physical Review Letters **131**, 068201 (2023).
[6] I. Grobas, M. Polin, and M. Asally, Elife **10**, e62632 (2021).
[7] G. O'Toole, H. B. Kaplan, and R. Kolter, Annual Reviews in Microbiology **54**, 49 (2000).
[8] N. C. Heer and A. C. Martin, Development **144**, 4249 (2017).
[9] S. G. Krens and C.-P. Heisenberg, Current topics in developmental biology **95**, 189 (2011).
[10] E. F. Teixeira, C. P. Beatrici, H. C. Fernandes, and L. G. Brunnet, Physical Review Letters **134**, 138401 (2025).
[11] M. Bothe, E. Lardet, A. Poliakov, G. Pruessner, T. Bertrand, and I. Bordeu, arXiv preprint arXiv:2503.13714 (2025).
[12] E. Méhes, E. Mones, V. Nemeth, and T. Vicsek, PloS one **7**, e31711 (2012).
[13] F. Leyvraz, Physics Reports **383**, 95 (2003).
[14] A. Nakajima and S. Ishihara, New Journal of Physics **13**, 033035 (2011).
[15] P. Cremer and H. Löwen, Physical Review E **89**, 022307 (2014).
[16] M. Durand, Plos Computational Biology **17**, e1008576 (2021).
[17] Y. Jiang and F. Leyvraz, Journal of Physics A: Mathematical and General **26**, L179 (1993).
[18] P. L. Krapivsky, S. Redner, and E. Ben-Naim, *A kinetic view of statistical physics* (Cambridge University Press, 2010).
[19] E. Mones, A. Czirók, and T. Vicsek, New journal of physics **17**, 063013 (2015).
[20] P. Baconnier, O. Dauchot, V. Démery, G. Düring, S. Henkes, C. Huepe, and A. Shee, Reviews of Modern Physics **97**, 015007 (2025).
[21] J. M. Belmonte, G. L. Thomas, L. G. Brunnet, R. M. C. de Almeida, and H. Chaté, Phys. Rev. Lett. **100**, 248702 (2008).
[22] T. Paul, N. Vadakkayil, and S. K. Das, Physical Review E **109**, 064607 (2024).
[23] C. P. Beatrici, R. M. de Almeida, and L. G. Brunnet, Physical Review E **95**, 032402 (2017).
[24] M. v. Smoluchowski, Z. Physik. **17**, 585 (1916).
[25] B. Szabo, G. Szöllösi, B. Gönci, Z. Jurányi, D. Selmeczi, and T. Vicsek, Physical Review E **74**, 061908 (2006).
[26] T. Vicsek, A. Czirók, E. Ben-Jacob, I. Cohen, and O. Shochet, Physical review letters **75**, 1226 (1995).
[27] S. Henkes, Y. Fily, and M. C. Marchetti, Physical Review E—Statistical, Nonlinear, and Soft Matter Physics **84**, 040301 (2011).
[28] D. Sarkar, G. Gompper, and J. Elgeti, Communications Physics **4**, 36 (2021).
[29] D. L. Barton, S. Henkes, C. J. Weijer, and R. Sknepnek, PLoS computational biology **13**, e1005569 (2017).
[30] A. Martín-Gómez, D. Levis, A. Díaz-Guilera, and I. Pagonabarraga, Soft matter **14**, 2610 (2018).
[31] Y. Zhao, T. Ihle, Z. Han, C. Huepe, and P. Romanczuk, Physical Review E **104**, 044605 (2021).
[32] See Supplemental Material at [URL will be inserted by publisher] for videos and analytical details, which includes Refs. [13, 17, 18, 23, 24, 40–42].
[33] F. Peruani, J. Starruß, V. Jakovljevic, L. Søgaard-Andersen, A. Deutsch, and M. Bär, Physical review letters **108**, 098102 (2012).
[34] Y. Fily and M. C. Marchetti, Physical review letters **108**, 235702 (2012).
[35] Y. Fily, S. Henkes, and M. C. Marchetti, Soft matter **10**, 2132 (2014).
[36] M. C. Marchetti, Y. Fily, S. Henkes, A. Patch, and D. Yllanes, Current Opinion in Colloid & Interface Science **21**, 34 (2016).
[37] A. Villa-Torrealba, C. Chávez-Raby, P. de Castro, and R. Soto, Physical Review E **101**, 062607 (2020).
[38] P. de Castro, S. Diles, R. Soto, and P. Sollich, Soft Matter **17**, 2050 (2021).
[39] M. Kolb, Physical review letters **53**, 1653 (1984).
[40] A. Moncho-Jordá, F. Martínez-López, M. Quesada-Pérez, M. Cabrerizo-Vílchez, and R. Hidalgo-Álvarez, Surface and Colloid Science , 113 (2004).
[41] A. Moncho-Jordá, F. Martınez-López, and R. Hidalgo-Álvarez, Physica A: Statistical Mechanics and its Applications **282**, 50 (2000).
[42] A. Moncho-Jordá, G. Odriozola, F. Martınez-López, A. Schmitt, and R. Hidalgo-Álvarez, The European Physical Journal E **5**, 471 (2001).
[43] O. Cochet-Escartin, T. T. Locke, W. H. Shi, R. E. Steele, and E.-M. S. Collins, Biophysical journal **113**, 2827 (2017).
[44] D. A. Beysens, G. Forgacs, and J. A. Glazier, Proceedings of the National Academy of Sciences **97**, 9467 (2000).